

Assembly and Characterization of a Flying Phase Retarder

Gabriel Bueno de Moraes Fior¹, Maxim Polikarpov²

¹ *Federal University of São Carlos, UFSCar, Brazil*

² *National Research Nuclear University (MEPhI), Moscow, Russia*

Supervisor – S. Francoual, J. Stremper



DESY, HASYLAB group
September 6th, 2012
DESY Summer Students Program 2012

Contents

| | | |
|------|---|----|
| 1. | Abstract..... | 2 |
| 2. | P09 beamline at Petra III, DESY..... | 2 |
| 3. | Assembly of the phase retarder..... | 3 |
| 4. | Diamond Phase plates..... | 4 |
| 4.1. | Orientation of diamond plates using back-scattering Laue diffraction | 4 |
| 4.2. | Determination of the mosaicity of diamond plates (Bragg diffraction) | 8 |
| 5. | Polarization analysis..... | 10 |
| 6. | Perfect crystals as phase retarding plates..... | 13 |
| 7. | Polarization experiment at 11.2 keV (Pt LIII-edge)..... | 18 |
| 7.1. | Circular polarization at 11.2 keV | 18 |
| 7.2. | Characterization of the degree of circular polarization | 19 |
| 8. | Summary about FPR (properties, construction disadvantages, list of improvements) .. | 22 |
| 9. | Multiple beam diffraction..... | 23 |
| 10. | Conclusions..... | 29 |
| 11. | References..... | 29 |

1. Abstract

Beamline P09 at PETRA III, DESY, is designed for general diffraction and resonant X-ray scattering experiments at low temperatures and high magnetic fields. The dependence of the X-ray cross-sections (Thomson, non-resonant magnetic, resonant exchange scattering, ATS) on the polarization state of the incident X-rays is an important property that one might want to capitalize on in a diffraction experiment. To that purpose, P09 is equipped with a double phase retarder setup [1] and diamond phase-plates making for the production of linearly and circularly polarized X-rays in the energy range between 3.5 and 8.5 keV as yet. The current phase retarder at P09 is located in the optic hutch in a UHV vacuum tank; because of this location the diamond plates it is equipped can't be easily changed. Here we describe a setup of the Flying Phase Retarder (FPR) at P09, which will be used to accommodate plates for the higher energy range, until 12 keV. This phase retarder is intended to be used either in the 1st or the 2nd experimental hutch. Its principles of operation and its performances with respect to the generation of circularly polarized X-ray beam using two eighth-wave plates in series or a single quarter-wave plate, will be explained.

2. P09 Resonant Scattering and Diffraction beamline at PETRA III, DESY : beamline layout

P09 is designed to operate in the hard x-rays regime with energies ranging from 2.7 to 50 keV. The beamline is located at Sector 6 of the PETRA III experimental hall and serves 3 experimental stations. The beamline consists of three experimental hutches. The first two experimental hutches, EH1 and EH2, are dedicated to resonant x-ray scattering and general diffraction (**RSD**) experiments. The third hutch, EH3, houses a Hard X-ray Photoelectron Spectroscopy (**HAXPES**) setup.



3. Assembly of the phase retarder

The flying phase-retarder is shown in Figure 3.1. The FPR consists of one Eulerian cradle, χ , which is equipped with two small ϕ goniometers such that $\Delta\chi = \chi_{2\text{nd goniometer}} - \chi_{1\text{st goniometer}} = 90$ degrees. A pitch and a yaw rotation underneath further help aligning the whole assembly precisely along the beam axis. The ϕ , χ , yaw and pitch rotations are motorized. Additional degree of freedom (e.g. z-axis of height of the phase plate) can be obtained by using goniometer heads to install the phase plates on the ϕ circles. Those additional degrees of freedom are manual translations and rotations. The FPR was mounted and now sits on the optic table in the experimental hutch 1 of P09 (Figure 3.2).

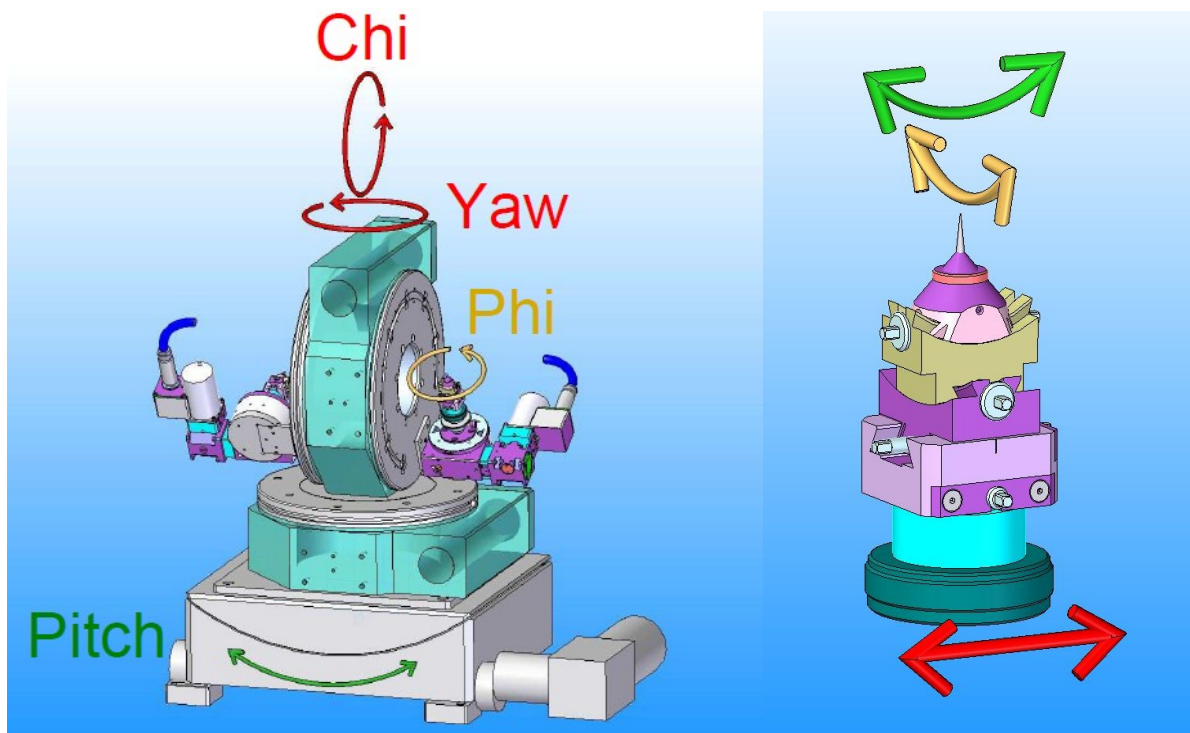


Figure 3.1. Flying phase-retarder at P09 (see text) and image of the goniometer head.

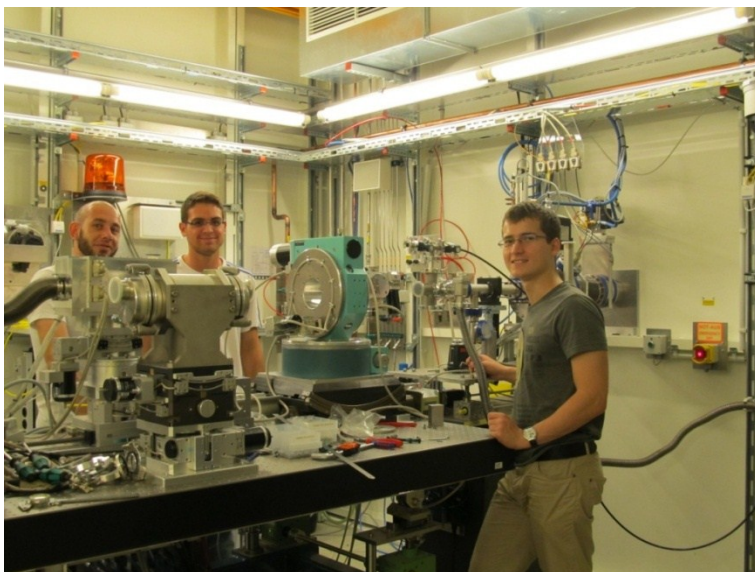


Figure 3.2.

FPR on the optic table in experimental hutch 1 at P09.

4. Diamond Phase plates

Two type-1b diamond crystals with thicknesses 680 and 640 μm s. were chosen for installation on the FPR (Figure 4).



Figure 4. Diamond crystals on goniometer heads

4.1. Orientation of diamond plates using back-scattering Laue diffraction

Back-scattering Laue diffraction method was used in the orientation of diamond plates. X-rays for this experiment were produced by X-ray tube at Laue laboratory at HASYLAB, DESY. The voltage and the current were set as 25 keV and 25 mA, respectively. These voltage and current were chosen specially for the diamond to give good resolution to Laue patterns.

Laue method is the following. The incoming beam, which has a continuous spectrum, hits the sample, reflects back from diffractions planes of the crystal and leaves marks the image plate (Figure 4.1). Due to the fact the beam has a spectrum of various wavelengths, different diffraction conditions can be satisfied at the same time, which leads to the set of spots on the image plate. These images are different for each reflection (which is perpendicular to the incident beam) and also called Laue maps. This maps are widely known for most of crystals and can be found elsewhere.

The goals of our experiment with diamonds were to check if the (1,0,0) reflection is parallel to the surface as it was expected; to find (1,1,1) reflection, and to make an orientation of crystals.

All procedures were made absolutely the same way for both crystals and here we will show them for the 2nd crystal (680 μms) as an example.

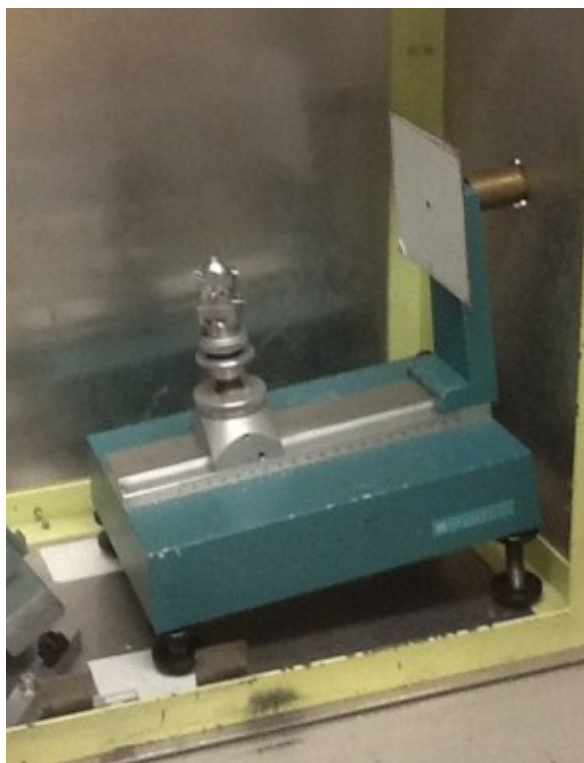


Figure 4.1. Photo of the setup for the back-scattering Laue diffraction, HASYLAB, DESY.

First of all, the diamond crystal was set on the goniometer so that its surface is perpendicular to the beam. So, if $(1,0,0)$ reflection is parallel to the surface, we should see Laue map for this reflection. We made a shot (Figure 4.1.2) and it is clearly seen from the picture that this is $(1,0,0)$ reflection, whose typical image can be found elsewhere. It is widely known that the diamond has a cubic structure. Moreover, on Figure 4.2, set of points which corresponds to $(0,1,1)$ reflection is the straight vertical line. This means that by rotation on $54,7$ degrees by clockwise (angle between $(1,0,0)$ and $(1,1,1)$ reflections) in plane, which is parallel to the table, we can get $(1,1,1)$. So, we set the position for $(1,1,1)$ and made another shot (Figure 4.3). It should be noticed here that we made offset 56 degrees instead of 54 , because we wanted to see the position of the central spot, but anyway by comparing with typical Laue map for $(1,1,1)$ for diamond, we confirmed our suggestion that this is $(1,1,1)$ reflection. Thereby, $(1,1,1)$ reflection was founded.

Then, alignment procedures were done. The essence of this procedures was to set the diamond so that the central spot would be independent of rotations between $(1,0,0)$ and $(1,1,1)$. This means that rotation occurs only in plane, which is parallel to the table, while all other degrees of freedom remains the same. Results are shown on Figures 4.4 and 4.5 and it is clearly seen that the central spot stays on the same position, which corresponds to the well alignment.

The same procedures were done for the first crystal.

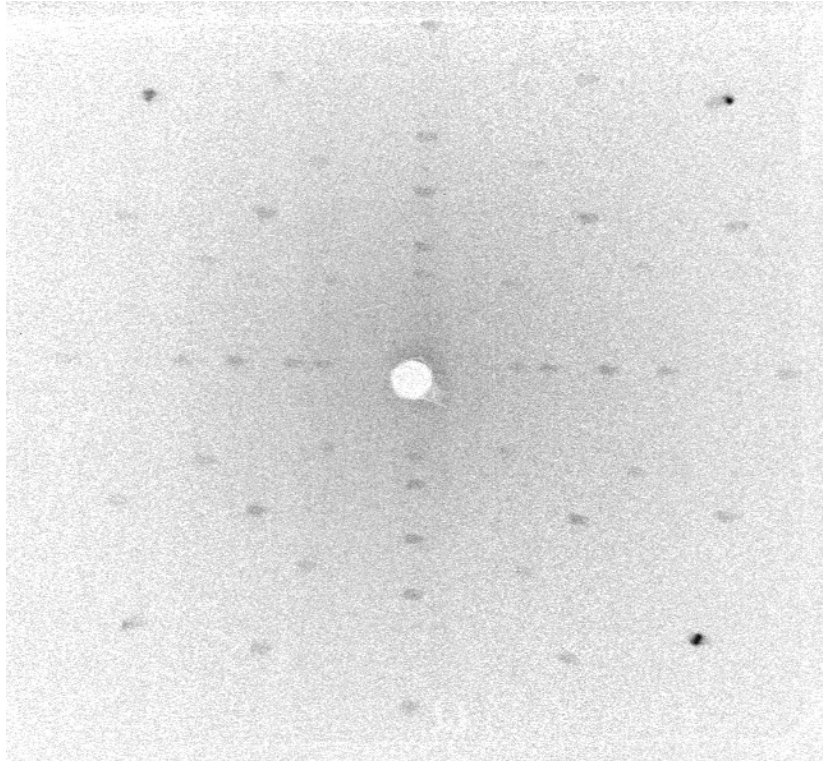


Figure 4.2. (1,0,0) reflection for the diamond crystal (680 μms).

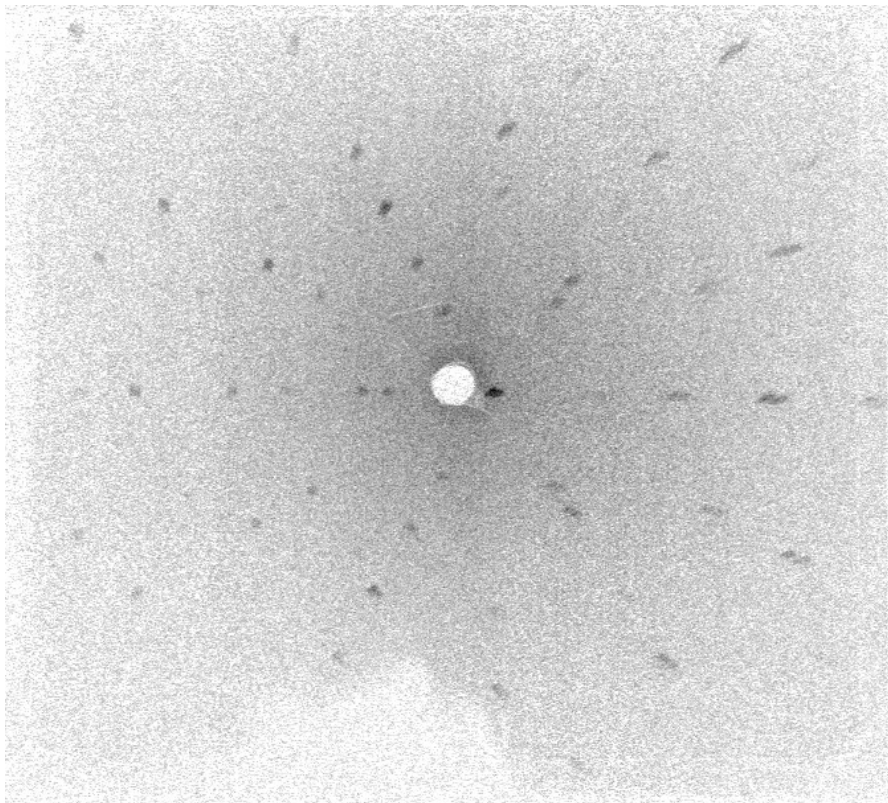


Figure 4.3. (1,1,1) reflection for the diamond crystal (680 μms).

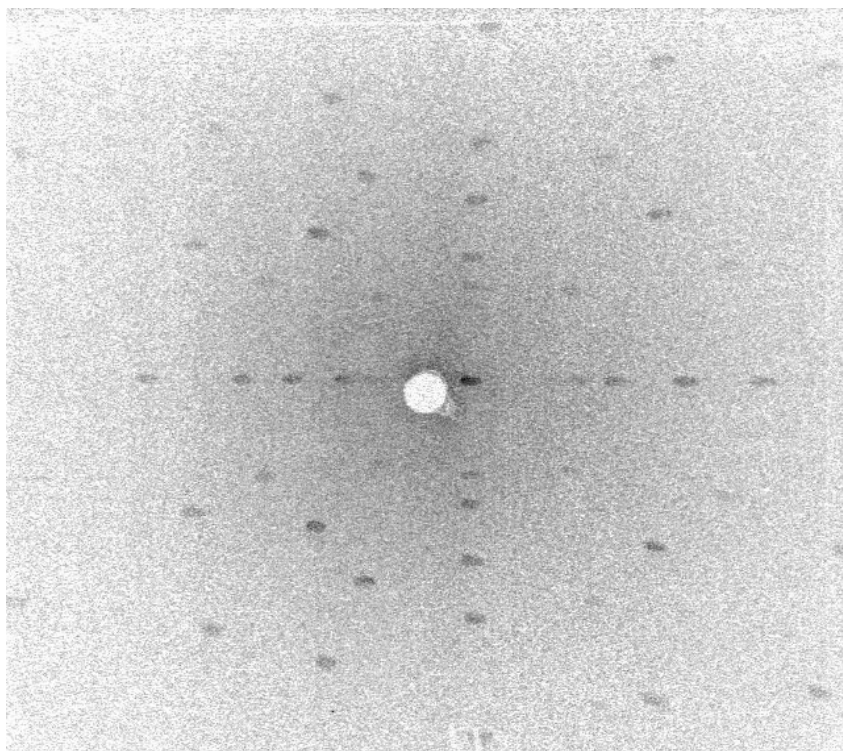


Figure 4.4. (1,0,0) plane for the diamond crystal (680 μms)

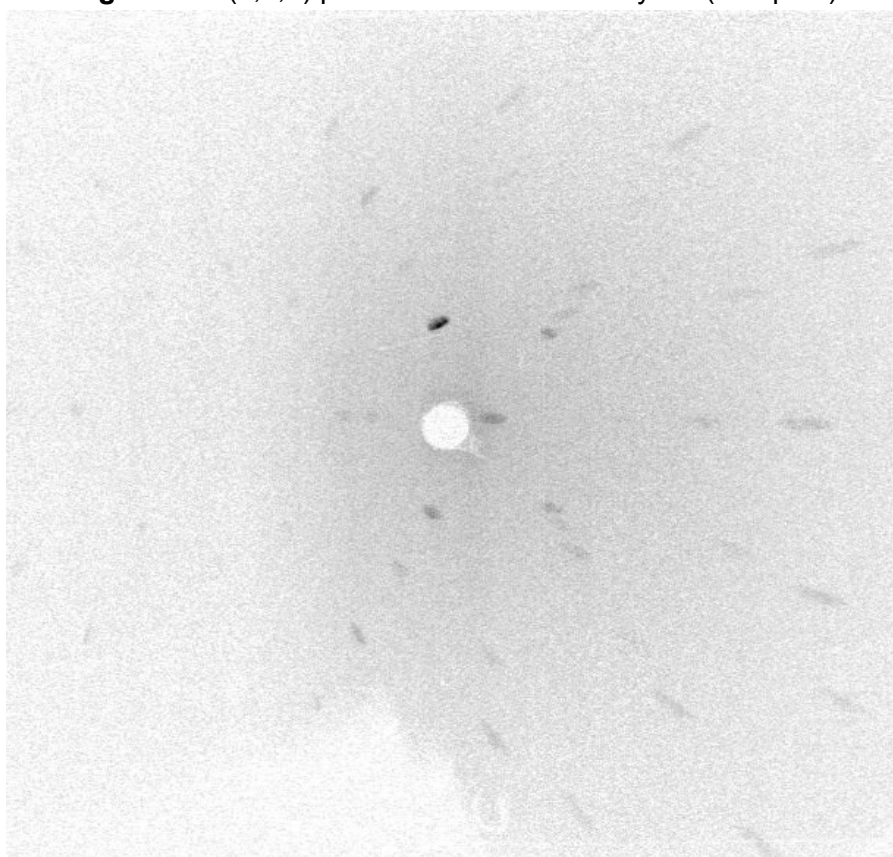


Figure 4.5. (1,1,1) plane for the diamond crystal (680 μms)

4.2 Determination of the mosaicity of diamond plates (Bragg diffraction)

4.2.1. Bragg diffraction introduction

Widely known kinematic X-ray theory tells us about principles of Bragg diffraction [3]. The Bragg law $n\lambda = 2d\sin\theta_B$, where λ – is a wavelength of the incident beam, d – interplanar distance between diffraction planes in the crystal, and θ_B – is the Bragg angle (Figure 4.6). You can see from this formula that for each energy there is only one Bragg angle, so, we should expect Intensity dependence of the diffracted beam on the θ angle as the delta function.

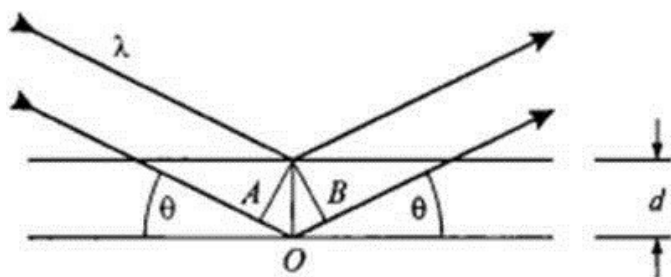


Figure 4.6. Diffraction of a plane wave off successive crystal planes. Strong diffraction results when the angles of incidence and diffraction, θ , are equal and the path difference AOB between the two beams is equal to $n\lambda$, an integral number of wavelength. Hence the Bragg law, $n\lambda = 2d\sin\theta$.

But real experiments showed that if we rock the θ angle near the Bragg condition, we will get the Gaussian distribution dependence instead of the delta function, which can be explained by dynamical theory of X-rays [7]. This real rocking curve usually has the width, which depends on the number of factors. Crystal defects (such as mosaicity, dislocations, etc.) are in list of this factors.

Nowadays diamonds for the electronic industry are created with almost perfect structure, but despite this fact some mosaicity might remain.

The goal of the current short experiment was to determine the mosaicity of the two 600 μm plates we want to use as phase-retarding plates.

4.2.2 The experiment

To measure the mosaicity of our diamond crystals, we did a high resolution diffraction experiment at experimental hutch 1 at P09.

First of all, some tuning of the beam and optics at the P09 was done. Energy was set at 8 keV. The beam was focused during the experiment and the beamsize was set as 200 μm .

The experiment was done in the Bragg diffraction geometry and the penetration depth of the beam was enough to see mosaicity influence on the rocking curve.

The diamond crystal plate is mounted on the 6 circles psi diffractometer in the vertical scattering geometry ($\chi \sim 180^\circ$, θ fixed). Experiment consisted at finding the (1,1,1) and (2,0,0) reflections and align the two reflections carrying out successive 2θ , χ and ϕ scans so as to define a UB orientation matrix. The rocking curve of the (1,1,1) and (-1, -1, 1) was then measured. Results are shown on Figure 4.2.2 and full width at half maximum (FWHM) for each curve is displayed in the inset. FWHM was obtained by fitting experimental data sets with Gaussian distribution.

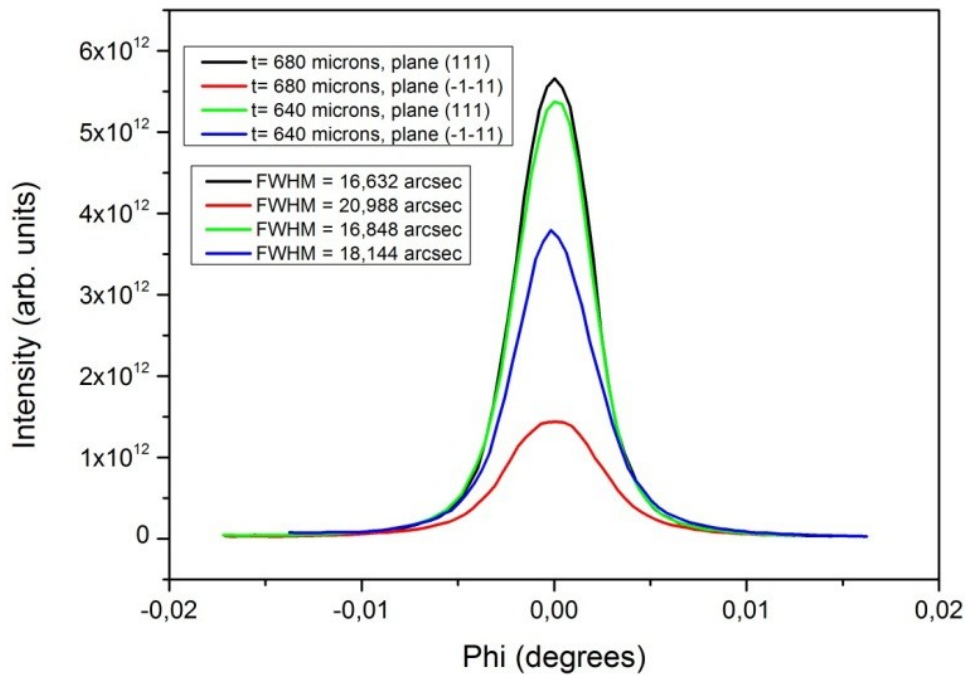


Figure 4.7. Experimental rocking curves for the diamond crystal 1 ($t = 680 \mu\text{m}$) and the diamond crystal 2 ($t = 640 \mu\text{m}$) for both (1,1,1) and (-1,-1,1) reflections.

It is clearly seen from the Figure 4.7, that broadening of the peak caused by mosaicity are 16.6 and 16.8 arcseconds for the first and the second crystal, respectively, at (1,1,1) reflection. This is larger than the Darwin width (the theoretical, ideal value for the full width at half maximum (FWHM)) for the (1,1,1) diamond rocking curve, which equals to 5.8 arcseconds. This means that mosaicity is present.

5. Polarization analysis

5.1. Polarization of light

The main reason for the development of a phase retarder lies on the possibility of control the polarization of the light of the incoming beam. It is also necessary to characterize the degree of polarization of the incoming beam and we explain here shortly how this is done.

X-Rays are transverse electro-magnetic waves, just like visible light, so that the description of polarized optics in the visible regime may be applied [4]. Electromagnetic waves travel in vacuum with the speed of light, and are composed by an electric- and a magnetic field. They are always perpendicular to each other and to the direction of the propagation of the beam. On Figure 5.1 we show a plane linearly polarized wave.

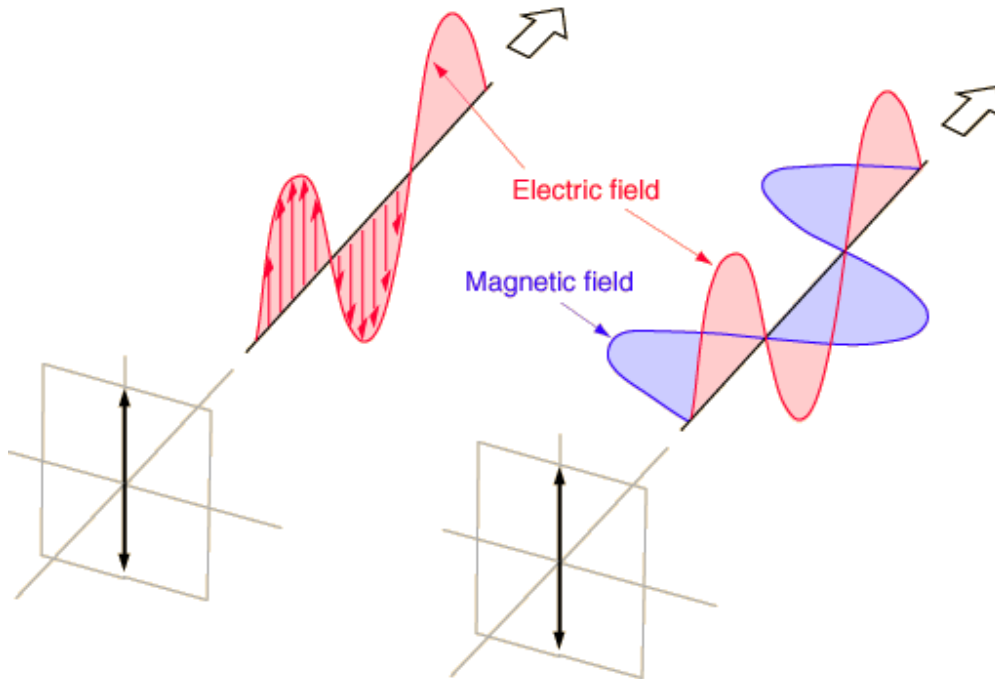


Figure 5.1. – Drawing representing the description of an electromagnetic wave [5].

So, since both the electric and the magnetic field are orthogonal vectors, we can choose one of them to define our polarization vector. By convention, we define the polarization vector as the direction of the electric field of the light. In the case of Figure 5.1, the polarization is linear, but there also other possibilities, such circular and elliptical polarization.

The electric field ($\mathbf{E}(\mathbf{r},t)$ is a vector) of an isolated wave with wave vector \mathbf{k} and photon energy $\hbar\omega$ propagating along \mathbf{e}_3 can be written as:

$$E(\mathbf{r}, t) = \text{Re}[(V_1\hat{e}_1 + V_2\hat{e}_2) \cdot e^{-i(\omega t - \mathbf{k} \cdot \mathbf{r})}] \quad (5.1);$$

where the Jones vector $V = \begin{pmatrix} V_1 \\ V_2 \end{pmatrix}$ contains information about the amplitude and phase of the electric field in the plane (e_1, e_2) orthogonal to e_3 . The intensity of light is proportional to the sum $I = |V_1|^2 + |V_2|^2$.

The Poincaré-Stokes parameters are conventionally used to describe the polarisation state of light rather than the Jones vector:

$$P_1 = \frac{|V_1|^2 - |V_2|^2}{|V_1|^2 + |V_2|^2}$$

$$P_2 = \frac{|V_1 + V_2|^2 - |V_1 - V_2|^2}{2(|V_1|^2 + |V_2|^2)}$$

$$P_3 = \frac{|V_1 - iV_2|^2 - |V_1 + iV_2|^2}{2(|V_1|^2 + |V_2|^2)}$$

The parameters P_1 and P_2 describe the state of linear polarization, and P_3 the degree of circular polarization, with $P_3 = +1$ for left-handed circular polarization. In addition, we define the degree of linear polarization as $P_{lin} = \sqrt{P_1^2 + P_2^2}$, $\mathbf{P} = (P_1, P_2, P_3)$ is called the Poincaré-Stokes polarization vector, although it does not have the transformation properties of a vector ($P_{1,2}$ have even parity, while P_3 has odd parity. An isolated photon is 100% polarized with

$$P = \sqrt{P_1^2 + P_2^2 + P_3^2} = 1 \quad (5.2)$$

5.2. Polarization analysis

Since we determined Stokes parameters, we can be reasonably questioned, what if we want to measure them. The polarization analysis method, which was showed in [2] can be applied.

In polarization analysis experiment we usually have incoming linear or circular polarized light and polarization analysis is making by rocking η axis (which is in plane, perpendicular to the beam) around the beam. And for each η value we are rocking the polarization analyzer crystal near its Bragg peak (Figure 5.2). From this procedure we can obtain Integrated intensity dependence of rocking the analyzer crystal on each value of η . And It can be shown that the integrated intensity of the scattered beam through a rocking of the analyzer crystal angle writes as a function of η , P_1 and P_2 as:

$$I = I_0 (1 + \cos^2(2\theta) + P_1 \cos(2\eta) \sin^2(2\theta) + P_2 \cos(2\eta) \sin^2(2\theta))$$

Here it is necessary to say few words about a polarization analyzer. Usually it is crystal (Thomson scatterer) with $2\theta_B = 90^\circ$. The $2\theta_B$ should be strictly 90 degrees to provide the possibility of rotation by angle η about the beam axis without losing Bragg diffraction conditions. In table 1 different analyzer crystals for different energies are performed.

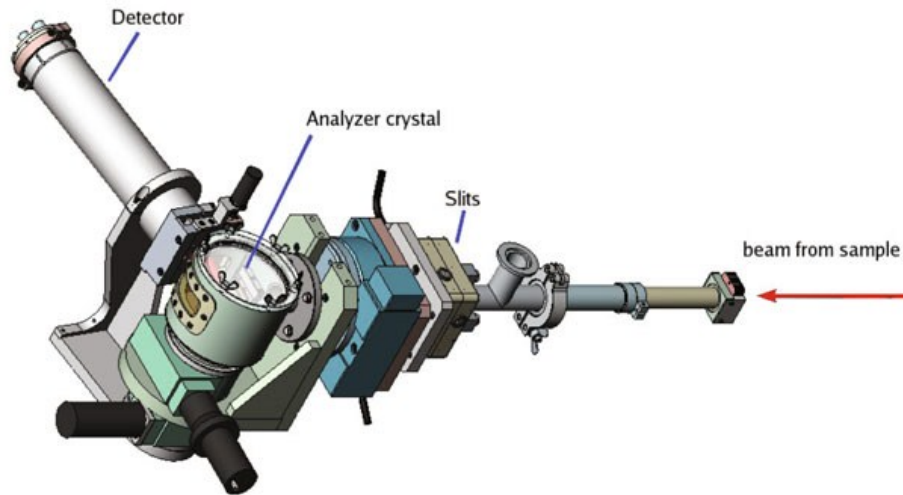


Figure. 5.2. Experimental configuration for linear polarization analysis of X-rays at the ESRF Beamline ID20 [26]. The beam scattered off the sample enters an evacuated flight tube (right). In-vacuum slits are positioned upstream of the analyzer crystal. The analyzer crystal and detector are mounted on a common goniometer rotating about the beam (η -axis). The Bragg (θ_{PA}) and scattering angles ($2\theta_{PA}$) can be adjusted individually. Set-up for polarisation analysis is similar at P09. The analyzer crystal has however additional χ and height degrees of freedom (attocube piezo stages). “C.Detlefs, M.Sanchez, C. Mazzoli Eur. Phys. J. Special Topics 208, 359-371 (2012)”

Table 1. A selection of crystals that can be used for polarization analysis from. The photon energy at which $2\theta_{PA} = 90^\circ$ is presented in column 3, while columns 4, 5 and 6 list some absorption edges for which the corresponding crystal represents a good choice.

| Crystal | (H K L) | d [Å] | $E(90^\circ)$ [keV] | Edges | | |
|----------|---------|----------|------------------------|---------------------|------------------------|--------|
| | | | | 5f M _{4,5} | 4f L _{1,2,3} | 3d K |
| Au | (1 1 1) | 2.355 | 3.72 | U, Np | | |
| Pt | (1 1 1) | 2.266 | 3.87 | | | |
| Cu | (2 0 0) | 1.807 | 4.85 | | | Ti |
| Graphite | (0 0 4) | 1.677 | 5.22 | | | Ti, V |
| Mo | (2 0 0) | 1.574 | 5.57 | | La, Ce | V |
| Al | (2 2 0) | 1.432 | 6.12 | | La, Ce, Pr, Nd | Cr, Mn |
| Cu | (2 2 0) | 1.276 | 6.86 | | Sm, Nd, Eu | Mn, Fe |
| Au | (2 2 2) | 1.177 | 7.44 | | Sm, Eu, Gd | Fe, Co |
| Al | (2 2 2) | 1.169 | 7.49 | | Sm, Eu, Gd | Fe, Co |
| Pt | (2 2 0) | 1.133 | 7.74 | | Sm, Eu, Gd, Tb, Dy | Co |
| Graphite | (0 0 6) | 1.118 | 7.84 | | Eu, Gd, Tb, Dy, Ho | Co |
| Cu | (2 2 2) | 1.042 | 8.41 | | Gd, Tb, Dy, Ho, Er, Tm | Ni, Cu |
| Pt | (4 0 0) | 0.981 | 8.94 | | Tb, Dy, Ho, Yb | Cu |
| Pd | (4 0 0) | 0.973 | 9.01 | | Tb, Dy, Ho, Yb | Cu |
| Graphite | (0 0 8) | 0.839 | 10.48 | | Tm, Yb, Lu | Zn, Ga |
| Au | (3 3 3) | 0.785 | 11.16 | | | Ge |

6. Perfect crystals as phase retarding plates

At X-Ray wavelengths, near Bragg reflections, perfect crystals are birefringent. The two orthogonal σ and π components of the electric field of the incident plane wave propagate through the crystal with different velocities and emerge phase shifted. This means that different phase shifts can be obtained by variation of the angular offset from the Bragg angle.

When the diffracting planes and the electric vector (polarization vector) present a 45° angle, the dynamical theory of X-rays show that the phase shift can be written as [10-12]:

$$\phi_{\sigma\pi} = -\frac{\left(\frac{\pi}{2}\right)r_e^2 \lambda_x^3 \text{Re}(F_G F_{-G}^*) \sin(2\theta_B) t_{eff}}{\Delta\theta (\pi V)^2} \quad (6.1);$$

where $\Delta\theta$ is the angular offset from the Bragg condition, $\phi_{\sigma\pi}$ is the phase shift between σ and π components of the outcoming beam, and t_{eff} is the effective thickness, which is determined by equation:

$$t_{eff} = t / \sin(\theta_G) \quad (6.2);$$

where t – thickness of the crystal, θ_G – glancing angle.

Usually it is said that the plate is half-wavelength when the phase shift is π , quarter-wavelength - when it is $\frac{\pi}{2}$, one-eighth wavelength - when it is $\frac{\pi}{4}$, etc.

The plates are used in transmission geometry. In our project, we mainly wanted to provide circular left- or right-handed polarization, which means that total phase shift must be $\pm \frac{\pi}{2}$. In that case, Eq. (6.1) shows the value of $\Delta\theta$ as a function of energy (proportional to λ), so that we can make a graph correlating both quantities (Figure 6.2).

It should be noted, that glancing angle for the (1,1,1) reflection plane for a (1,0,0) plate is determined as $\theta_G = 54.7356 \pm \theta_{Bragg}$, where 54.7356 is separation in angle between the (1,1,1) and (1,0,0) reflections and θ_{Bragg} is the Bragg angle for the (1,1,1) reflection. “+” and “-” are cases when the beam is coming from different sides of the (1,1,1) plane (Figure 6.1).

Another analysis, which was made with MATLAB®, was to determine the transmission rates for the plates, for the entire energy range of operation, which can be seen in Figure 6.3.

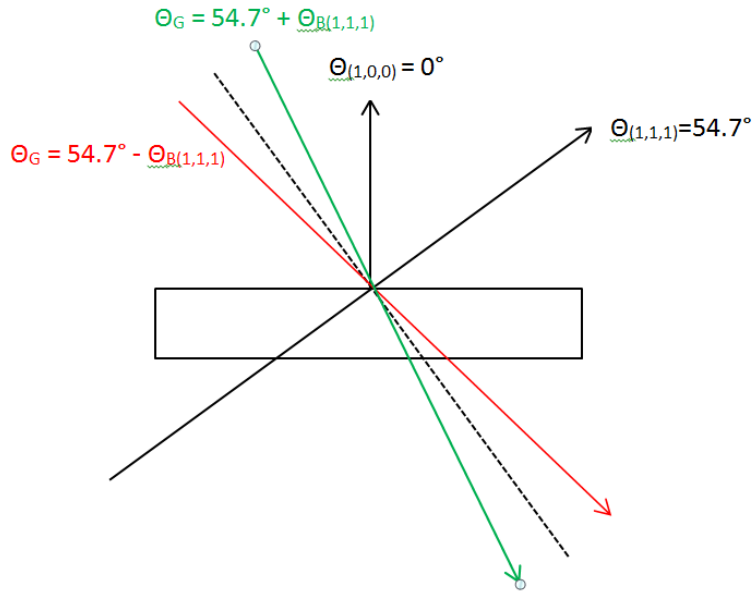


Figure 6.1. Schematic drawing of different glancing angles for (1,1,1) reflection. In case of “+”, beam path through the crystal is shorter, which corresponds to low absorption and therefore higher transmission rate than in case of “-”.

The transmission rate is an important parameter to consider : it is acceptable to work down to transmission rates of 10% to 20 % (i.e. the incident flux is reduced by a factor 10 going through the plates); lower transmission rates are not affordable especially for magnetic scattering experiments where intensity at peak might be as slow as 20 to 100 cts/ s. The lower transmission rate defines the lower energy at which we can work with one finite thickness of the plates. For instance here with the 600 microns plates from Figure 6.3. 20% transmission rate brings ~7 keV as the lowest energy at glancing angle $\theta_G = 54.7356 - \theta_{\text{Bragg}}$ and ~8.5 keV at glancing angle $\theta_G = 54.7356 + \theta_{\text{Bragg}}$.

Following conclusions can be made from Figures 6.2 and 6.3:

- 1) The higher the energy, the lower the angular offset from Bragg peak. Good degree of polarization can be obtained when we are working far from total Bragg diffraction. The mosaicity defines the higher energy at which we can work. The 600 μm s plates have FWHM ~20" and it is safe to work at deviation angles $\Delta\theta > 3 \cdot \text{FWHM} / 2 \sim 30''$. For quarter-wave plate condition from Figure 6.2 we can work up to ~9.5 keV using the plate such that the glancing angle is $\theta_G = 54.7356 - \theta_{\text{Bragg}}$ and up to ~10.5 keV when the glancing angle is $\theta_G = 54.7356 + \theta_{\text{Bragg}}$.
- 2) For “-” case of the glancing angle, angular offset is bigger, while for “+” case, transmission rate is bigger.

From 1) and 2), we need a kind compromise between the transmission rate and the angular offset conditions to have a successful experiment. The most comfortable energy range to work is from 7 to 10 keV for a phase shift of $\frac{\pi}{2}$. But what if we want higher energy range? We can use two one-eighth plates with phase shift $\frac{\pi}{2}$ for each plate while the total phase shift will be $\frac{\pi}{2}$ (Figure 6.4).

From figure 6.4 you can see angular offsets curves here for 1/8 WP and 1/4 WP. For the 1/8 WPs case the angular offset 30" is on 11.5 keV for "+" case of glancing angle and at 12keV for "-" case of glancing angle, respectively. This means that condition is more comfortable for us in comparison with 1/4 WP.

So, we can use two crystals in 1/8 condition to get 1/4 WP total condition while we will be working on higher angular offsets which is more comfortable. And it should be mentioned here, that in case of two plates, absorption increases which leads to decreasing of the transmission rate. For example, if you have transmission rate 30% for only one plate, you will get only 10% of incident intensity after using two crystals.

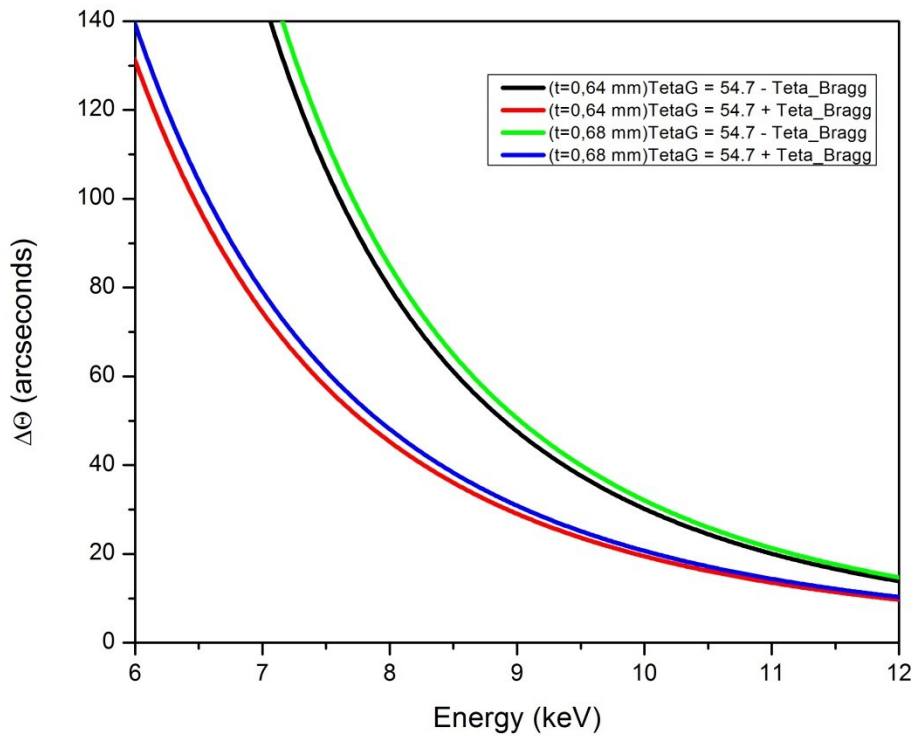


Figure 6.2. Energy dependence of the Quarter Wave Plate (QWP) condition for diamond plates (1,0,0) 640 and 680 μ m thick.

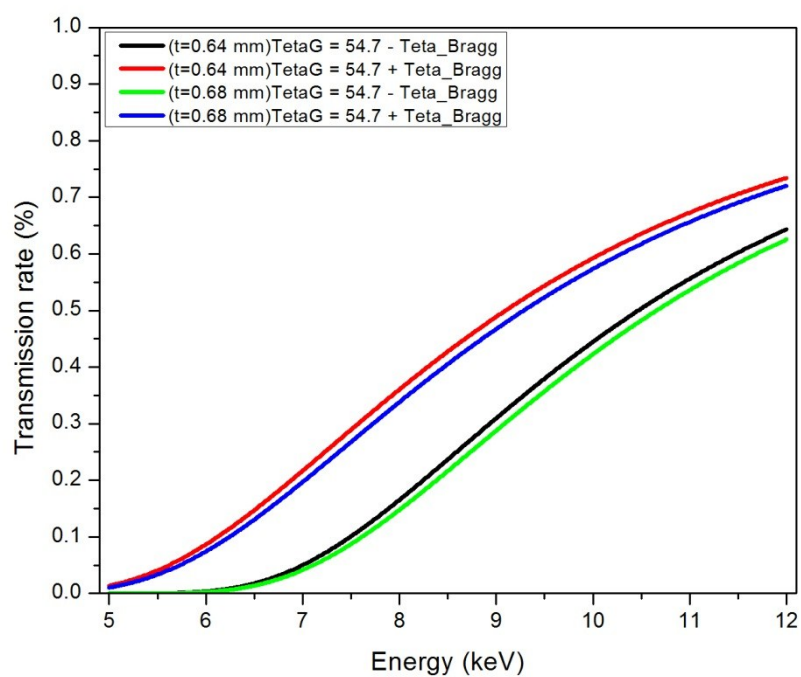


Figure 6.3. Energy dependence of the Transmission Rate for diamond plates (1,0,0) 640 μm and 680 μm thick.

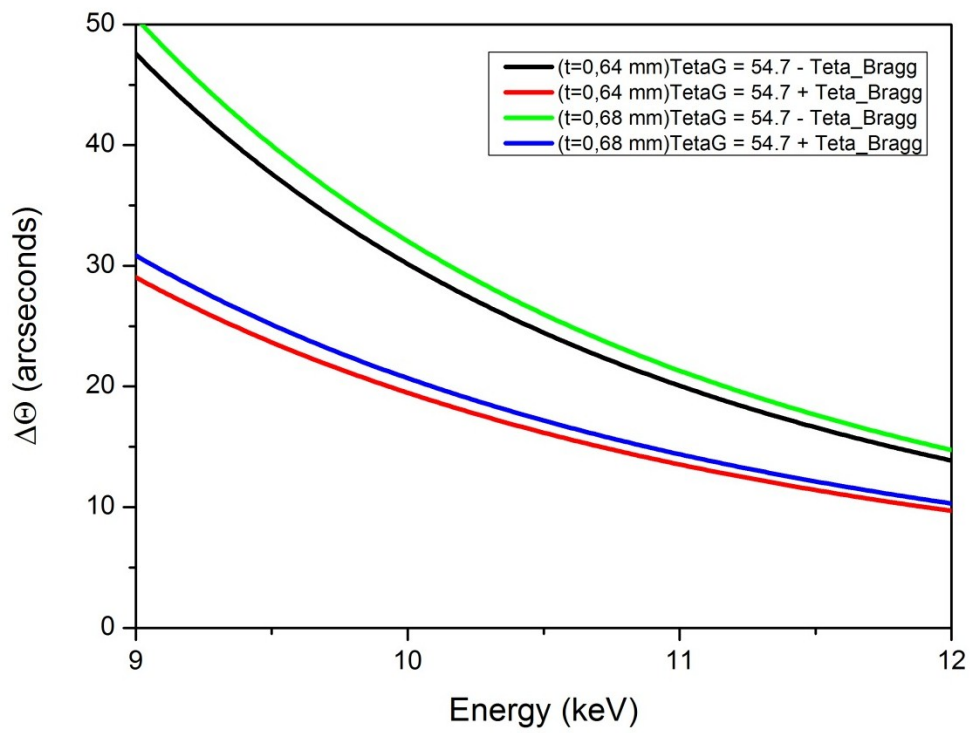
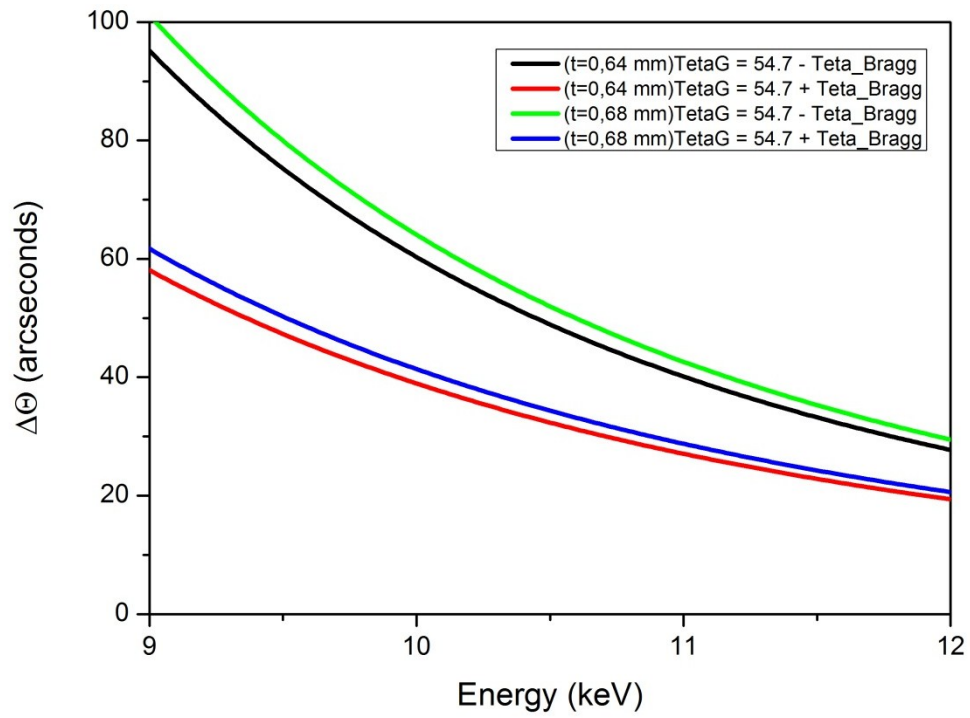


Figure 6.4. Deviation angle dependence on energy for 1/8 WP (top) and for 1/4 WP (bottom)

7. Polarization experiment at 11.2 keV (Pt L_{III}-edge)

7.1. Circular polarization at 11.2 keV

To provide circular polarization at 11.2 keV we had to use two 1/8 wave plates rather one plate (was discussed in paragraph 6). Working with one single plate acting as quarter-wave plate, from figure 6.4, angular offset would be 14". This is too close to total Bragg diffraction. One has then to use two 1/8 wave plates as two 1/8WPs in series allows it to generate circular polarization. 1/8 wave plate is such that $\Delta\theta_{1/8WP} = 2 \Delta\theta_{1/4WP}$ which allows it to work outside the range of total Bragg diffraction. The two 600 μms plate were mounted on the flying phase retarder and aligned so that glancing angle on the (111) plane is $54.356 + \theta_{\text{bragg}}$ and the two plates act as 1/8 wave-plate i.e. $\Delta\phi = \pi/8$.

It should be mentioned here that we did checking of our Matlab calculations (week before this experiment), in which we went to the (1,1,1) Bragg condition for the first diamond (680 μms) at 10.5 keV and rocking curves of the diamond at σ - σ ($\eta=0^\circ$) and σ - π ($\eta=-90^\circ$) were done. Images were obtained and shown on Figures 7.1, 7.2.

By calculating the distances between two main peaks (and dividing by two) on each image, we obtained the angular offset ($\Delta\theta_{\text{experim}} = 28''$) for the quarter-wavelength plate, which coincided with our Matlab calculations ($\Delta\theta_{\text{matlab}} = 26''$).

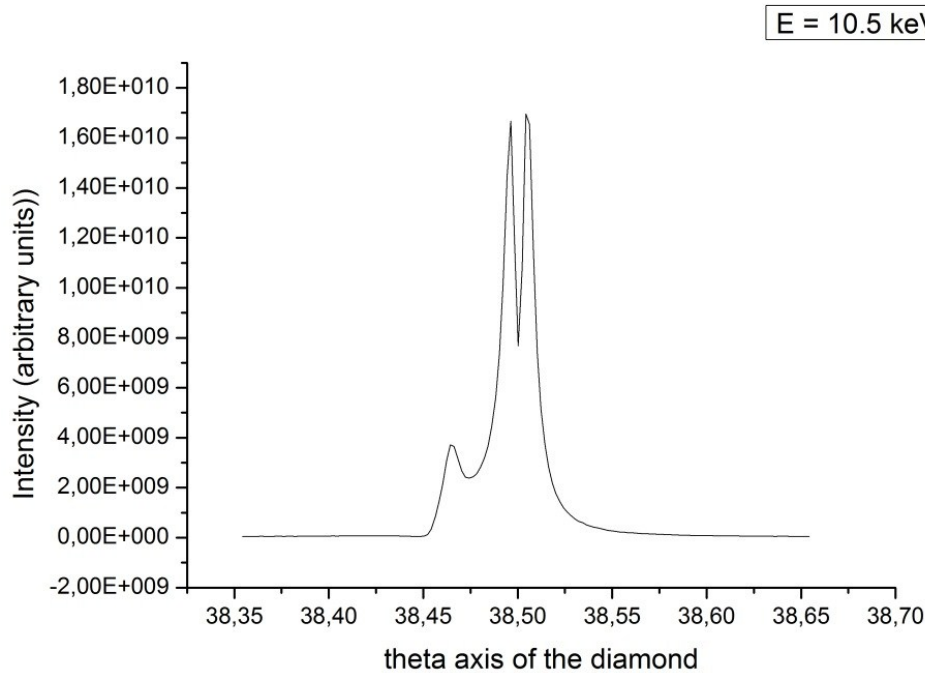


Figure 7.1. Rocking curve of the 1st diamond crystal at $\eta=-90^\circ$

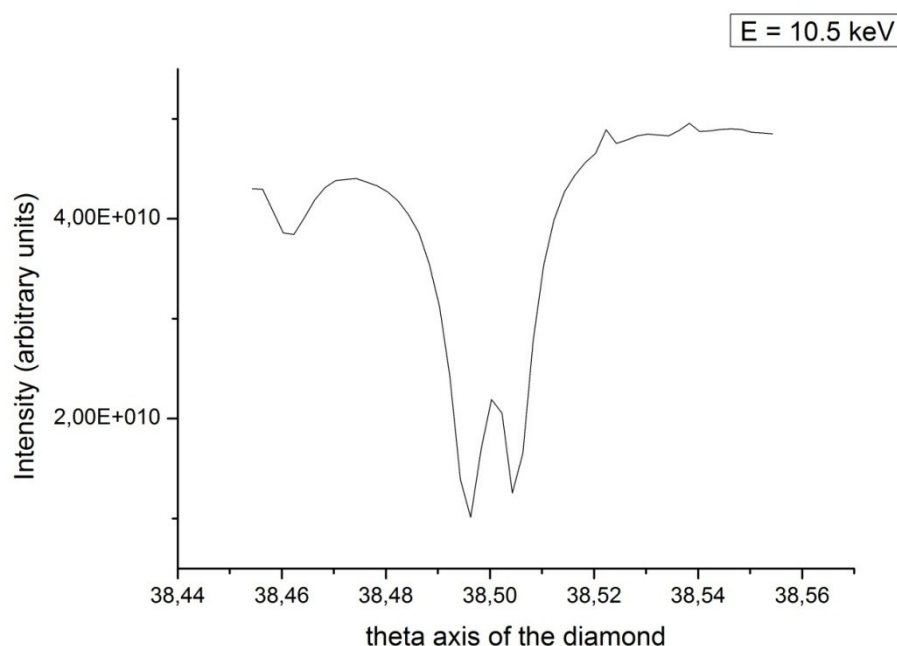


Figure 7.2. Rocking curve of the 1st diamond crystal at $\eta=0^\circ$

7.2. Characterization of the degree of circular polarization

The analyzer (Al 333) was selected as the most appropriate at this energy and diffraction conditions for the analyzer were found. As it has been mentioned before (in paragraph 5.2) the PA crystal's is selected such that the scattering angle $2\theta \sim 90^\circ$ at the working energy. In our case for Pt L_{III} - edge energy $2\theta_B$ is not exactly 90° but 87.4° . Figure 7.3. shows the rocking curve of the analyzer. It is easily seen that there are two peaks, which tells about bad quality of the crystal and large mosaicity.

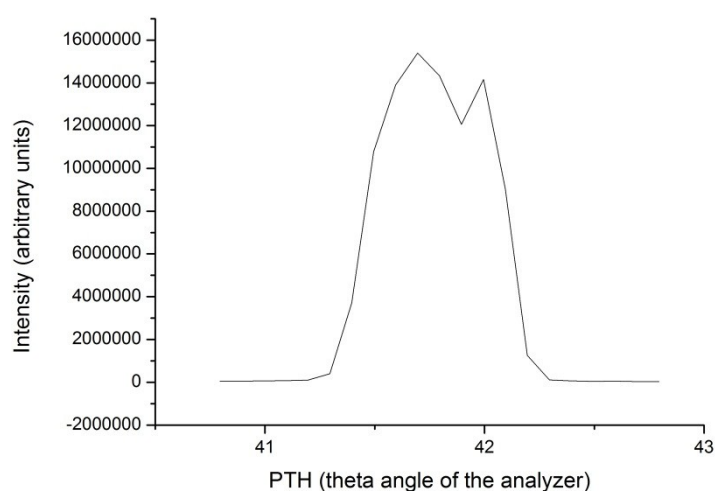


Figure 7.3. Rocking curve of the analyzer crystal Al 333; Scattering angle $2\theta=87.4^\circ$

We were trying to do polarization analysis (as it was discussed at paragraph 5.2) with this analyzer but it turned out that the rocking curve was different at different η position which is not acceptable for a good polarization analysis.

So we decided to use Au 333 as the analyzer. Bragg conditions and rocking curves for gold were obtained and are shown on Figure 7.4. It is clearly seen that gold has sharp rocking curve with single peak, which can allow us use it as analyzer.

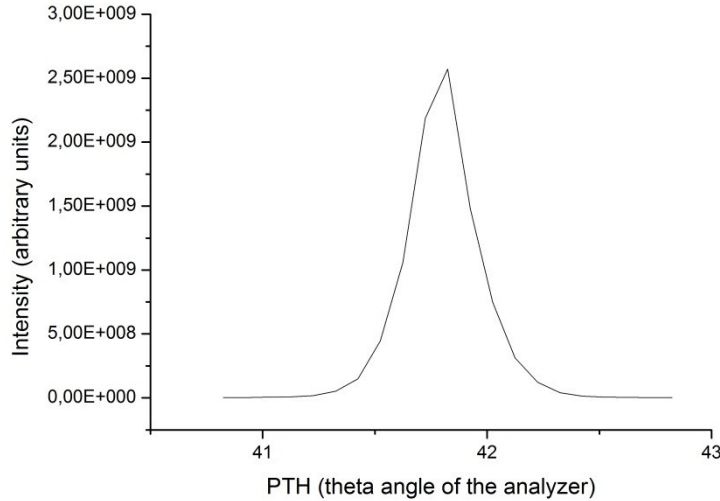


Figure 7.4. Rocking curve of the analyzer crystal Au 333; Scattering angle $2\theta = 86.3^\circ$

Polarization analysis was done for circular left- and right-handed polarized light obtained using the two 600 μms plates at 1/8 wave plate condition. Integrated intensity were obtained using DIFFIT program and $I(\eta)$ curves were fitted with Origin 8.6 using equation

$$I = I_0 (1 + \cos^2(2\theta) + P_1 \cos(2\eta) \sin^2(2\theta) + P_2 \cos(2\eta) \sin^2(2\theta))$$

The fitted curves are shown Figures 7.5 and 7.6. Determined Stokes parameters P_1 , P_2 and P_3 are shown in table 2 where we assume that amount of unpolarized light $P_{\text{un}} = 0$, which means that P_3 can be determined from equation

$$P = \sqrt{P_1^2 + P_2^2 + P_3^2} = 1$$

Table 2: Stokes parameters of the circularly polarized light

| | Circular left-polarized light | Circular right-polarized light |
|-------|-------------------------------|--------------------------------|
| P_1 | -0.13 ± 0.02 | -0.19 ± 0.03 |
| P_2 | 0.02 ± 0.02 | 0.01 ± 0.02 |
| P_3 | 0.991 ± 0.003 | 0.981 ± 0.006 |

Conclusions of the polarization analyzer experiment:

1) Figures 7.5 and 7.6 shows almost linear intensity dependence on η angle, which means that we obtained a good degree of circular polarization.

2) Stokes parameters P_1 , P_2 , P_3 were determined which says us that this method can be used for determination of polarization parameters at P09. P_3 parameter is more than 0.98 which also can tell us about good degree of circular polarization.

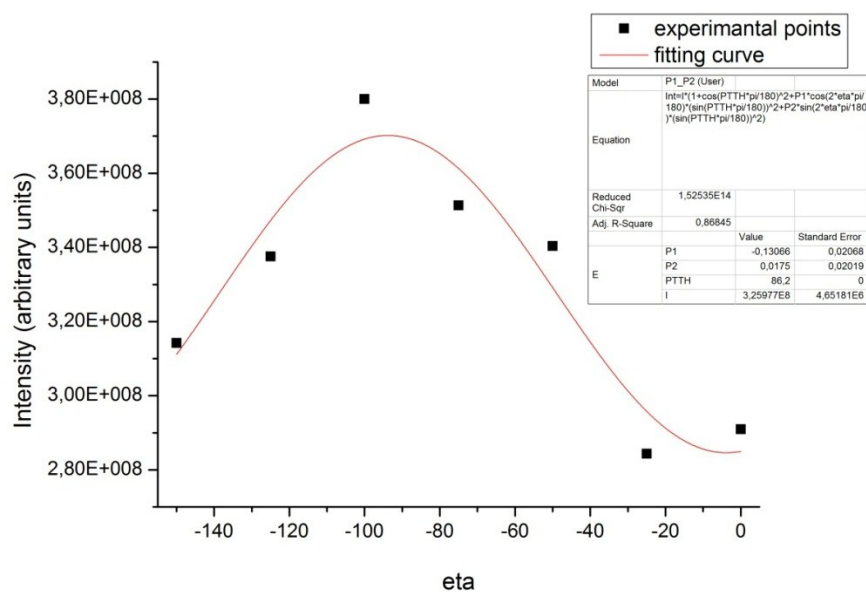


Figure 7.5. Polarization analysis for the circular left-handed polarized light

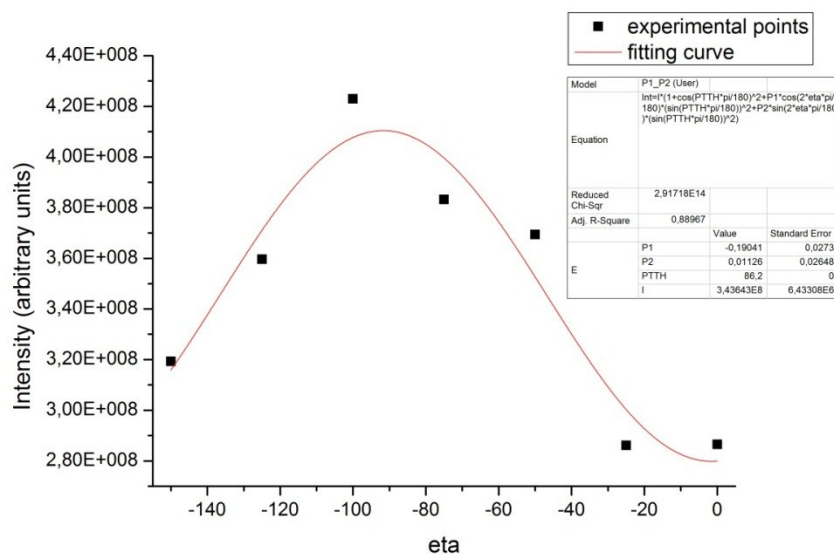


Figure 7.4.6. Polarization analysis for the circular right-handed polarized light

8 Summary about FPR (properties, construction disadvantages, list of improvements)

In this section we present the current status of the Flying Phase Retarder in the Experimental Hutch 1 at the beamline P09 at Petra III.

The current phase retarder is just a prototype. Part of our project was to study the assembly of the device and to suggest improvements. In that sense, we concluded that there are 2 main improvements to be made:

1. Better control of the z-coordinate.

The position of diamond plates are controlled by 2 goniometer heads. We could not adjust the height of the goniometers on the ϕ stages at all. We propose to lower down the position of the ϕ circles on the χ circles (see figure 4.1) so that small z stages, enabling a ± 3 mm tolerance, can be used with the present goniometer heads to bring the plate at the center of the χ stage.

2. Reduce sphere of confusion of χ circle

During the FPR assembly process, it turned out that we have a large sphere of confusion in χ ($\sim 750 \mu\text{m}$) because of the big amount of screws and holes and the play between them. So, in order to reduce the sphere of confusion to acceptable values ($< 100 \mu\text{m}$), a pin positioning device has to be used. Moreover, we propose to reduce the number of parts and the number of holes / screws to a value as low as possible.

3. 1-piece two- ϕ circles stage

The two ϕ circles were found not to be at 90° in χ from each other, what is needed to guarantee the anti-parallel geometry. Because of that, we made a decision to develop a new one-piece goniometer supporter (Figure 8.1).

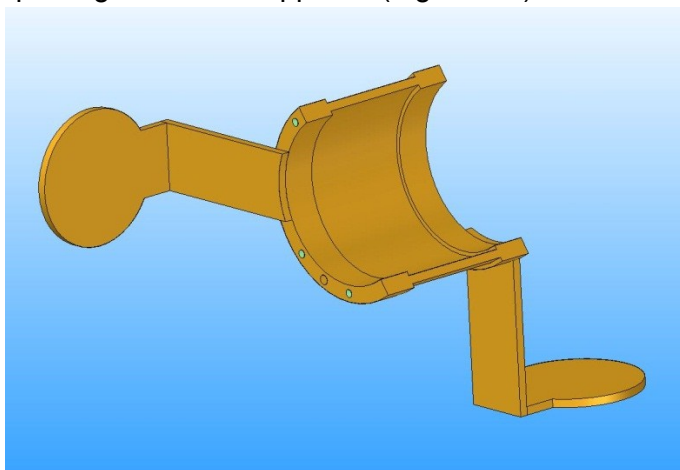


Figure 8.1. 1-piece composition of goniometer supporter for FPR.

4 Holder for the diamonds.

In our assembly process we had to align diamond crystals by back-scattering Laue diffraction method. This pre-alignment procedure was crucial as it allowed to save time at the beamline, since we already knew required tilts, as well as the exact angles of rotation to put the desired planes in diffraction.

Holders have to be machined to the shape of the plates so that the orientation found at the Laue is guaranteed and the plates can be mounted on the ϕ stages of the flying phase retarder without further time consuming alignment. A kinematic mount would be the best option.

9 Multiple beam diffraction

Many interesting and challenging studies in x-ray physics, such like XMCD and resonant magnetic scattering require an accurate knowledge on the polarization of an incident x-ray beam. It's therefore important to characterize the X-Ray polarization in a convenient and precise way.

As discussed before, the polarization of the light can be completely described by the normalized Stokes Parameters $P = (P_1, P_2, P_3)$. P_1 represents the degrees of the 0° and 90° (σ and π) linear polarization, while P_2 represents the degrees of the $+45^\circ$ and -45° linear polarization and P_3 - the degree of the circular left- or right-handed polarization, respectively [6].

In previous sections, we couldn't directly determine P_3 . What we did was to assume that the beam was completely polarized and the amount of unpolarized light $P_{un} = 0$. Then, P_3 was obtained by the relation $P_3 = 1 - \sqrt{P_1^2 + P_2^2}$. Unfortunately this relation is not always true. If a greater accuracy is needed, for example in the experiments quoted in the beginning of the section, it would be able to determine P_3 precisely.

The method that we'll go into details in this section is called Multiple Beam Diffraction (MBD), and occurs when two or more planes of the crystal satisfy simultaneously Bragg's Law.

A convenient way to achieve this condition of multiple scattering is to rotate the diffracting crystal around the scattering vector Q , described by an azimuthal angle ϕ , while always keeping one Bragg reflection excited ($H=Q$). The reflection H is called the main reflection and the reflection L is the detoured reflection. While on the multiple scattering condition, polarization mixing occurs, leading to a dependence between the intensity measured by the detector and the Stokes parameters P_1 , P_2 and P_3 .

$$I_{int} = I B(\phi) \{ \cos(\delta) [A_{\sigma\sigma} + A_{\pi\pi} \cos(2\theta)] + P_1 \cos(\delta) [A_{\sigma\sigma} - A_{\pi\pi} \cos(2\theta)] + P_2 \cos(\delta) [A_{\pi\sigma} + A_{\sigma\pi} \cos(2\theta)] + P_3 \sin(\delta) [-A_{\pi\sigma} + A_{\sigma\pi} \cos(2\theta)] \} \quad (9.1)$$

Since the intensities in equation 9.1 depend on all three Stokes Parameters, it's possible, using a known crystal, to determine \mathbf{P} . By reading reference [6], one can observe that Gallium Arsenide (GaAs) was successfully used, so we decided to repeat the experiment.

The procedure that we followed was started by aligning the GaAs single-crystal, by means of the Laue Back-Reflection technique. We knew that the direction normal to the surface was the (1,1,1), but we didn't know anything else. In the Laue technique, it's possible to easily rotate the sample, in order to bring in different planes into diffraction. This is possible because the sample is mounted in a goniometer head. Therefore, with the Laue procedure, after producing images, we were able to locate 2 diffraction planes, (1,1,1) and the (0,1,1).

In a second moment, we have gone to the beamline, and we assembled the GaAs in the diffractometer. The diffractometer can rotate the angles θ , 2θ , χ and Φ , as shown in the Figure 9.1.

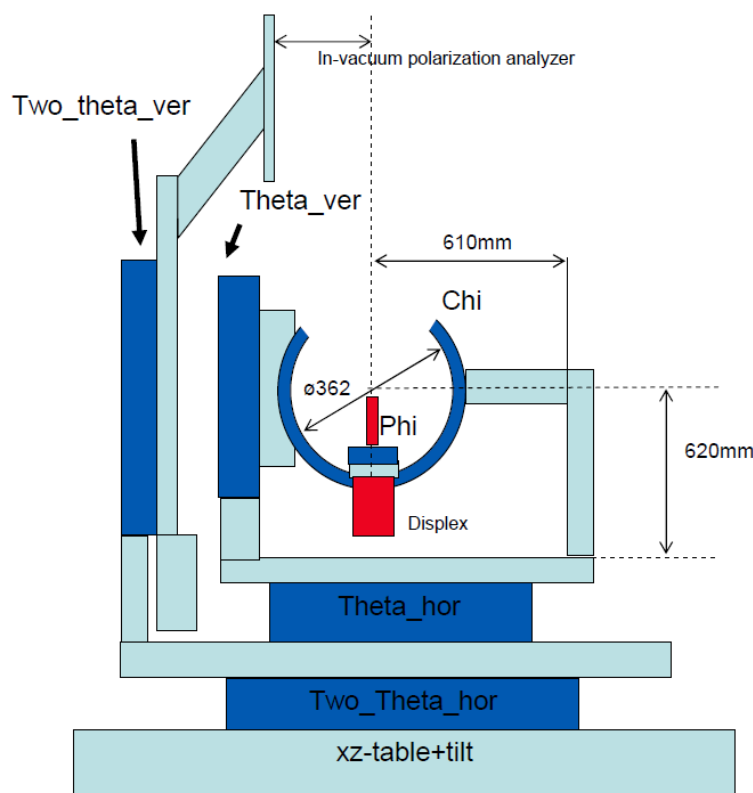


Figure 9.1. Schematic drawing of the diffractometer, illustrating the degrees of freedom of the sample holder.

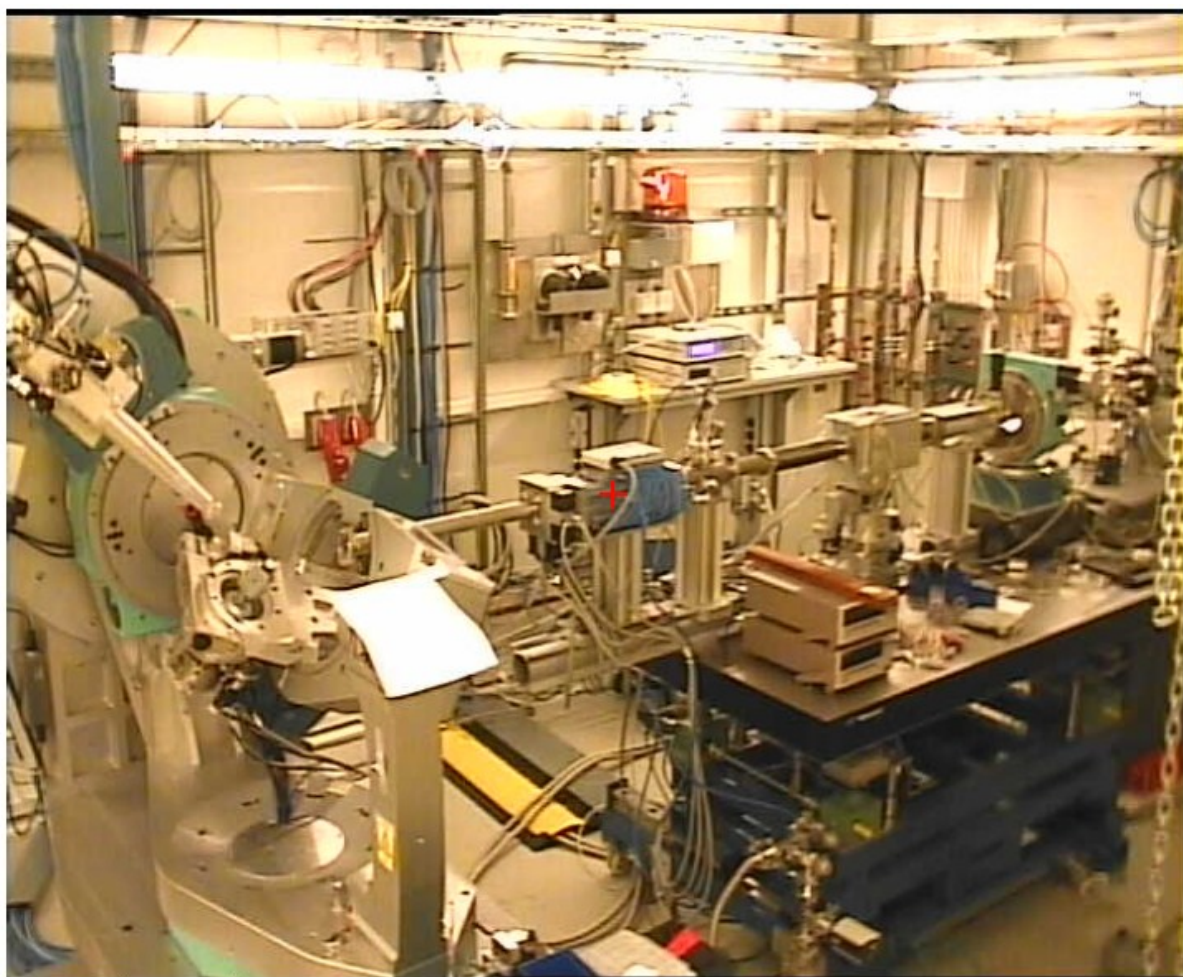


Figure 9.2 – Photo of the setup of beamline P09 at Petra III during the MBD Experiment.

The experiment was carried out at 8.076 KeV, because of two reasons. The first one is that a XMCD-type experiment was carried out at the Ho L_3 edge, for which it's necessary to know precisely the value of P_3 . The second reason is that Gallium Arsenide (GaAs) is the best crystal for a MBD experiment at 8 KeV since multiple scattering conditions are best separated as a function of ψ . This is shown in figure 9.3 [10]. GaAs, combined with the employed energy, provide a parameter (a/λ) of approximately 3.7, which is removed from the bottom region, where the separation between peaks is small. Nevertheless, at higher energies diamonds are the best choice.

Since we aligned the sample at the Laue, we were able to quickly reach the desired diffraction planes. After we have aligned the (2,2,2) and (0,2,2) Bragg peaks of the GaAs, we could define a UBmatrix, which is used by the diffractometer server together with the information about the sample structure (lattice parameters + angular symmetry). This is done to define the transformation between the diffraction space (position Q in reciprocal space) and the sample space (position in real space = diffractometer angles). From this analysis any Q position is calculated and can be automatically reached.

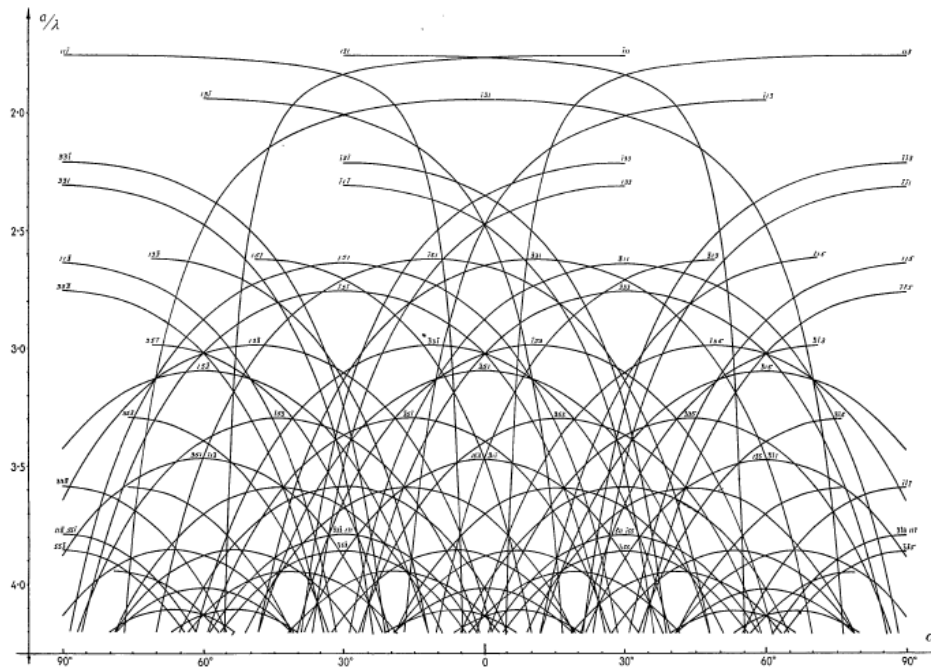


Figure 9.3 – Plot of (a/λ) versus ψ , the azimuthal angle of rotation. It represents the reflection peaks that come up during the psi scan for a crystal-like structure.

The (2,2,2) reflection is normal to the surface of the sample and was easy to align. Then, we made an azimuthal scan (ψ), trying to bring other diffraction planes into the Ewald Sphere. However the (2,2,2) reflection is very sharp (0.0037° rocking curve) and we had to rock θ for each value of ψ in order to keep the (2,2,2) in diffraction. It is worth remembering that all the procedures we followed were firstly proposed by [6].

MBD condition was obtained for $\psi = -84.78^\circ$ for which we had strong intensity. We rotated the sample by 90° in ψ to try to bring the (3,1,1) detoured reflection into diffraction which is expected for $\psi \sim -5.76^\circ$, but we didn't succeed finding it. We then did measurements at $\psi = -84.78^\circ$, which corresponds to the detoured reflection (3,5,1) / (-1,1,-3), according to [7].

Measurements consisted of making θ scans for different ψ angles within $\pm 0.5^\circ$ around the position $\psi = -84.78^\circ$. Each θ scan was later integrated, so that we have an integrated intensity for each ψ . Those θ scans were made by 2 different methods: fast scans and lup scans. The fast scan is faster, but noisier. It doesn't stop the detector at a specific point, it just keeps moving. The lup scan is less noisy, but much slower, since for each θ the detector stops, count the number of photons, and then move to the next position.

Later on, we centered and normalized the curve by the intensity far away from the MBD condition, and the profile obtained is shown in Figure 9.4.

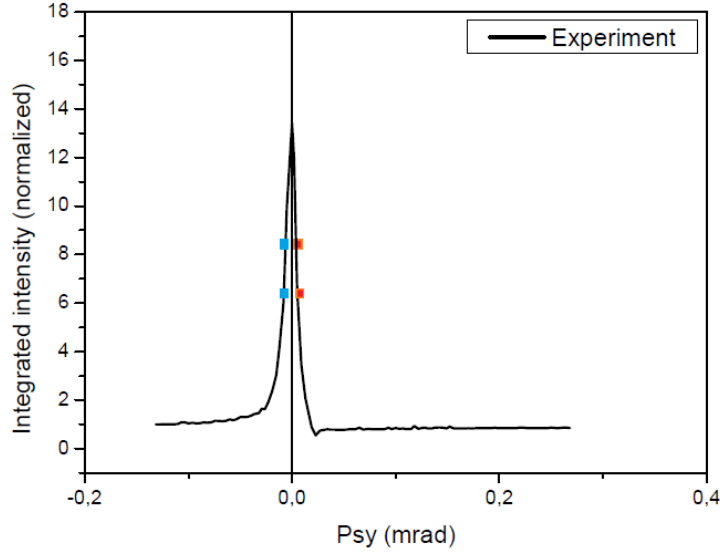


Figure 9.4. Relation between the integrated intensity and the ψ , for the azimuthal scan.

We made this procedure for the 3 polarization states of the incident light: linear, left- and right-handed circularly polarized light. The double-phase retarder in the optic hutch was used to produce circular polarization. In this case we used one single 400 μm diamond plate set at quarter wave plate (QWP) condition. For both cases where we had circularly polarized light, asymmetric profiles were obtained, on which you can see reversed asymmetry for circular left- and circular right-handed polarization. Moreover, no asymmetry is observed for the linear polarized case.

Afterwards, we subtracted the integrated intensity from symmetric points, as shown in figure 9.4. For points with the same offset from the center, we subtracted from the intensity of the point in the right in the graph (red) the intensity of its symmetric point in the left (blue). Therefore, we have an intensity difference for each value of $\Delta\psi$.

Following reference [6], we plotted the intensity difference versus the inverse of $\Delta\psi$, obtaining a linear trend for each of the 3 cases. The graphs can be found on figure 9.5.

One important result we obtained was that different signs of slopes were obtained for the circular left and circular right cases. This is an indication, following the guidance of reference [6], that our experiment was successful.

Right now analysis is not finished. We still have to calculate the coefficients $A_{\sigma\sigma}$, $A_{\pi\sigma}$, $A_{\pi\pi}$ and δHL in equation 9.1 and fit linear trend using equation 9.2.

$$I_{int} = I B(\phi) \{ \cos(\delta) [A_{\sigma\sigma} + A_{\pi\pi} \cos(2\theta)] + P1 \cos(\delta) [A_{\sigma\sigma} - A_{\pi\pi} \cos(2\theta)] \\ + P2 \cos(\delta) [A_{\pi\sigma} + A_{\sigma\pi} \cos(2\theta)] + P3 \sin(\delta) [-A_{\pi\sigma} + A_{\sigma\pi} \cos(2\theta)] \} \quad (9.2)$$

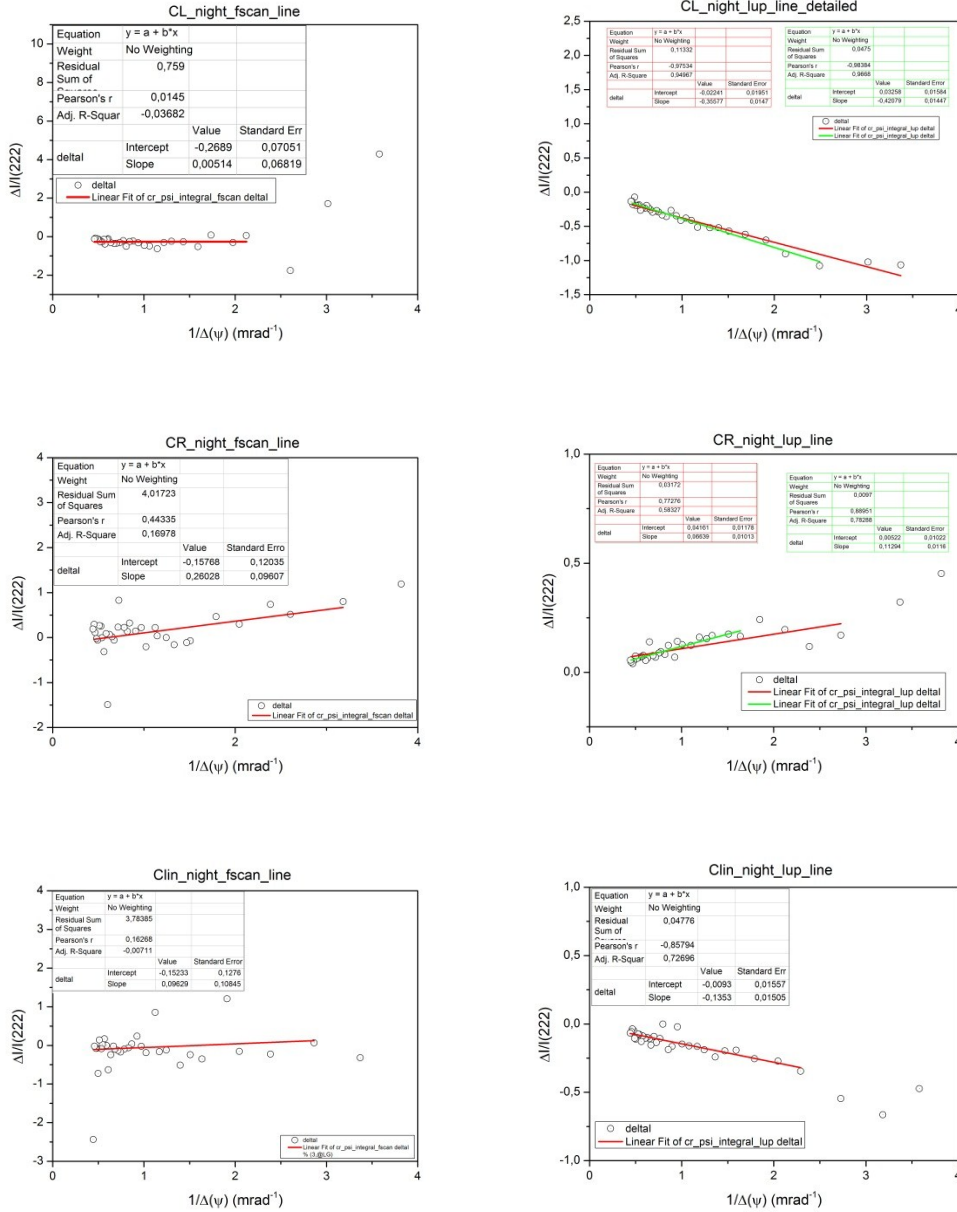


Figure 9.5. Relation between the difference in integrated intensity $\times 1/\Delta\psi$, for the 3 cases we analyzed. Top 2 graphs refer to the Circular Left case; the middle 2 refer to the Circular Right case; the bottom 2 graphs refer to the Linear case.

During the MBD experiment polarization analysis of the direct beam was carried out, using a graphite analyzer, in order to obtain P1 and P2. Hence we can reduce equation 9.2 to a simpler equation (equation 9.3), since only P3 is unknown. Another possibility is to work with a detour reflection like the (3,1,1) for which $\delta = 90^\circ$ and the equation is greatly simplified (equation 9.4), depending only on P3.

$$I_{int} = I B(\phi) \{ \cos(\delta) [A_{\sigma\sigma} + A_{\pi\pi} \cos(2\theta)] + P3 \sin(\delta) [-A_{\pi\sigma} + A_{\sigma\pi} \cos(2\theta)] \} \quad (9.3)$$

$$I_{int} = I B(\phi) \{ P3 \sin(\delta) [-A_{\pi\sigma} + A_{\sigma\pi} \cos(2\theta)] \} \quad (9.4)$$

10 Conclusions

At the end of our project, we were able to reach our goal, which was to assemble and to characterize a prototype flying phase-retarder.

In the Optics Hutch at P09 at PETRA III, there is a fixed Phase Retarder, which works in the energy range 3.5 – 8.5 KeV. It is important to have a different phase retarder for experiments at higher energy, until 12 KeV. With the setup we worked on, it was possible to generate a circularly polarized beam with a high degree of circular polarization ($P_3 > 0.9$) in energies up to 11.2 keV that before were unreachable. This set-up was used successfully during a user's experiment on 10th of august at P09.

Finally, since the current setup of the phase retarder is a prototype, we made a list of improvements for the next version.

Moreover, the MBD experiment we carried out was a first try experiment to determine P_3 by a direct method. The time allocated for that experiment was of only 8 hours, which was quite short considering the sharp rocking curve of the (2,2,2) reflection in GaAs. Results are however convincing and analysis needs to be completed.

11 References

- [1] Double phase-retarder set-up at P09, S. Francoual et.al., Submitted (Proceedings SRI 2012)
- [2] Scagnoli V, Mazzoli C, Detlefs C, Bernard P, Fondacaro A, Paolasini L, Fabrizi F and De Bergevin F, 2009 J. Synchrotron Rad. **16** 778
- [3] High resolution X-Ray Diffractometry and Topography – D. Keith Bowen and Brian K. Tanner 2005
- [4] C. Detlefs, M. Sanchez del Rio, C. Mazzoli. Eur. Phys. J. Special Topics. 208 359-371 (2012). DOI: 10.1140/epjst/e2012-01630-3
- [5] <http://hyperphysics.phy-astr.gsu.edu/hbase/phyopt/polclas.html#c1>
- [6] Q. Shen and D. K. Finkelstein, Phys. Rev. B 45(9) 1992
- [7] H. Cole, F.W. Chambers and H.M. Dunn, Acta. Crys. (1962). **15**, 138